ANL/MCT/CP--76348

DE93 002905

ANALYSIS OF LIQUID–SOLIDS SUSPENSION VELOCITIES AND CONCENTRATIONS OBTAINED BY NMR IMAGING

by

Jianmin Ding, Robert W. Lyczkowski,+ and William T. Sha,
ARGONNE NATIONAL LABORATORY
Materials and Components Technology Division
+Energy Systems Division
9700 South Cass Avenue
Argonne, IL 60439 USA

Stephen A. Altobelli, and Eiichi Fukushima
LOVELACE MEDICAL FOUNDATION
2425 Ridgecrest Drive, S.E.
Albuquerque, NM 87108 USA

Manuscript Submitted to
NSF/DOE Workshop on *Flow of Particles and Fluids*
September 17-18, 1992
National Institute of Standards and Technology
Gaithersburg, Maryland

September, 1992

ANALYSIS OF LIQUID-SOLIDS SUSPENSION VELOCITIES AND CONCENTRATIONS OBTAINED BY NMR IMAGING

by

Jianmin Ding, Robert W. Lyczkowski,+ and William T. Sha
ARGONNE NATIONAL LABORATORY
Materials and Components Technology Division
+Energy Systems Division
9700 South Cass Avenue
Argonne, IL 60439 USA

Stephen A. Altobelli and Eiichi Fukushima
LOVELACE MEDICAL FOUNDATION
2425 Ridgecrest Drive, S.E.
Albuquerque, NM 87108 USA

Abstract

COMMIX-M, a three-dimensional transient and steady-state computer program written in Cartesian and cylindrical coordinates, has been developed by Argonne National Laboratory. This computer program is capable of analyzing multiphase flow and heat transfer and utilizes the separate phases model wherein each phase has its own mass, momentum, and energy equations. This computer program is in its early stages of development for application to test various interphase interaction models and to predict design and processing of dense fluid-solids suspension systems. COMMIX-M contains preliminary constitutive relationships for interfacial drag, solids viscosities and stresses to describe the solids rheology, and shear lift forces from the literature. Also included is a solids partial slip boundary condition to allow non-zero tangential velocity at the tube walls. Analyses of some of the steady-state, fully-developed isothermal carrier fluid velocity and solids concentration data of Altobelli et al.[1] and Sinton and Chow[2] are presented. These experimental data obtained using three-dimensional time-of-flight nuclear magnetic (NMR) imaging techniques, were carefully performed, and represent some of the best available open literature data of their kind. NMR imaging offers powerful techniques to non-intrusively determine three-dimensional time-dependent velocity and concentration fields to assist development and validation of the constitutive models and the computer programs describing concentrated suspensions. Analyses of these NMR data, together with comparisons of computed and measured concentration and velocity profiles provide some insights into the mechanisms governing the observed phenomena. Recommendations for future research are given. To the authors' knowledge, these are the first such comparisons of theory and experiment.

1. Introduction

Argonne National Laboratory has initiated an in-house project in support of research on concentrated suspensions, usually called slurries. A coordinated methodology is being pursued involving theory (field and constitutive equation development), experimentation, and validation utilizing computer modeling. ANL anticipates that synergism will result when a conscious effort is made to coordinate the execution of this research program involving complex and interdisciplinary phenomena requiring advances both of a theoretical and experimental nature.

ANL's philosophy is to utilize a self-consistent methodology to link micro- and macro-fluid mechanical phenomena. This approach will ensure that the design and instrumentation of the experiments, the data acquisition and its processing for use in field and constitutive equation development, and computer code validation are on a one-to-one correspondence.

A great deal of theory has arisen over the last twenty years concerning multiphase modeling. The major thrust in the 1970s and early 1980s was research in the nuclear area. Bedford and Drumheller[3] have reviewed this area comprehensively, and possibly definitely in their 1983 article which addresses continuum theories of immiscible constituents. This theory, adopted in this paper, constitutes one class of approaches which have been investigated to develop multiphase flow models for dense suspensions.

Primarily independently, progress has been made in advancing dry and wet multiphase particulate flow modeling. Success can be achieved in this area if a coordinated and conscious effort is made to utilize a self-consistent methodology such as described above.

There have been prior efforts which have utilized this philosophy to study wet concentrated suspension. The work of Graham et al.[4-6] is one such example. They coupled stereoscopic split-screen video determination of three-dimensional particle locations[4] together with techniques derived from Maximum Entropy Principle (MEP), information, and cell theories to determine cluster shape and size distributions[5] and suspension viscosity.[6]

Concentrated suspensions flowing in conduits can exhibit nonhomogeneous temporal and spatial distributions of the suspended particles. For low shear-rate flows, this nonuniform distribution of particles results from hydrodynamic interactions between neighboring particles and the flow-confining boundaries. To understand the fundamental behavior of these flowing materials, and thereby construct engineering models, quantitative, noninvasive data are needed for constituent velocities and concentrations. Moreover, assessment of the flow-induced structure of the suspension is crucial for understanding the interactions between the carrier fluid and particles.

These velocity and concentration measurements, which are of intrinsic value to engineering design efforts, are difficult (and sometimes impossible) to make with existing noninvasive experimental techniques (e.g., gamma-ray attenuation, tracers, coherent laser light beams, ultrasound, and electrical impedance techniques). Some of these measurement techniques use focused light, sound waves, or ion beams, techniques which suffer signal attenuation due to opacity or scattering at nondilute particle concentrations (i.e., greater than a few percent). Nuclear magnetic resonance (NMR) techniques do not suffer from transmission effects in electrically nonconducting samples and can yield three-dimensional (3-D) velocity and concentration information in a single experiment. Additional research will further increase the spatial and temporal resolutions.

Several pulsed Fourier-transform NMR imaging strategies (see, for example, Wendt et al.[7] or Caprihan and Fukushima[8]) have been developed which yield spatially resolved velocity distributions of flowing fluids. Kose et al.[9] introduced two-dimensional (2-D) NMR flow-imaging techniques that result in both velocity profiles and flow-compensated concentration distributions. Caprihan et al.[10] developed a frequency-encoded one-dimensional (1-D) NMR technique that is expandable to 2-D and 3-D velocity distributions. All these techniques were developed for pure fluids and have very recently been applied to the flow of concentrated suspensions.

At Lovelace Medical Foundation, Altobelli et al.[1] and at Lockheed Palo Alto Research Laboratory, Sinton and Chow[2] have used 3-D NMR flow visualization techniques developed earlier by Kose et al.[9] and Majors et al.[11] to study nonuniform velocity and concentration profiles of small, negatively buoyant[1] and neutrally buoyant[2] particles respectively. Proton NMR signals were obtained using a transverse phase encoding gradient technique. Flow

velocity and concentration visualizations were obtained from the displacement of a tagged slice oriented perpendicular to the flow direction using fast Fourier reconstruction algorithms.

It is the purpose of this paper to present the analyses of the Altobelli et al.[1] and Sinton and Chow[2] experiments using the COMMIX-M computer program. The progress made to date and recommendations for future research are presented. A brief description of the computer code and the preliminary constitutive models employed are given, as are brief descriptions of the experiments performed.

2. Computer Model Description

We will use the computational framework of the COMMIX code. The COMMIX series of computer programs, developed at ANL over a nearly two decade time span, are mainly employed to perform steady-state and transient three-dimensional fluid flows with heat transfer in nuclear reactor systems. COMMIX solves a set of phasic equations of conservation of mass, momentum, and energy as a boundary value problem in space and an initial value problem in time[12]. The concepts of volume porosity, directional surface porosity, distributed resistance, and distributed heat source are used to facilitate modeling temperature and velocity field due to presence of internal solid structures and they can be readily used to approximate irregular geometries[13].

In these analyses, the in-house version of COMMIX-M is used. The formulation of the convective, diffusion, interfacial friction, and interfacial heat-transfer terms as well as additional source terms in the governing equations, are made implicit for a more stable formulation. The final form of all discretization equations is such as to permit various solution schemes.

The pressure-solution method of COMMIX used by deriving, through a combination of the momentum and continuity equations, a Poisson-like equation which describes the pressure distribution. The numerical solution of the pressure equation is obtained either with the iterative Successive Over-Relaxation (SOR) method or by means of a direct matrix inversion method which uses decomposition of the matrix of coefficients. The iterative method is most suitable for large-size problems, while the direct method is advantageous for small- and middle-size problems (typically, up to a thousand cells). The COMMIX code has a modular structure. It permits analysis of single-phase (gas or liquid) or multi-phase flow problems. These governing equations, preliminary constitutive equation, and boundary conditions used in COMMIX-M are now described below.

2.1 Governing Equations

The isothermal multiphase equations solved in COMMIX-M in three-dimensional Cartesian and cylindrical coordinates are given by:

Continuity

$$\frac{\partial}{\partial t}(\varepsilon_k \rho_k) + \nabla \cdot (\varepsilon_k \rho_k \vec{v}_k) = 0 \qquad (1)$$

Momentum

$$\frac{\partial}{\partial t}(\varepsilon_k \rho_k \vec{v}_k) + \nabla \cdot (\varepsilon_k \rho_k \vec{v}_k \vec{v}_k) = -\varepsilon_k \nabla P + \varepsilon_k \rho_k \vec{g}$$

Acceleration; Pressure Drop; Gravity

$$+ \sum_{i=1}^{M} \beta \cdot (\vec{v}_i - \vec{v}_k) + \nabla \cdot \bar{\bar{\tau}}_{ke} + \vec{F}_{kL} \qquad (2)$$

Interphase Drag; Stress Shear Lift

Note that both volume porosity and directional surface porosities are set to unity since no internal structures are involved here. In general, each phase is denoted by the subscript k and the total number of phases is M. The effective stress tensor $\bar{\bar{\tau}}_{ke}$ is composed of viscous and coulombic portions according to the convention[14-16]

$$\bar{\bar{\tau}}_{ke} = \varepsilon_k \bar{\bar{\tau}}_{kv} - \delta_{ks_f} \bar{\bar{\tau}}_{kc} \qquad (3)$$

Viscous; Coulombic

The sum of the phase volume fractions add up according to

$$\sum_{k=1}^{M} \varepsilon_k = 1 \qquad (4)$$

The microscopic viscous stress terms for each phase are given by

$$\bar{\bar{\tau}}_{kv} = 2\mu_k \bar{\bar{S}}_k. \qquad (5)$$

where the strain rate tensor is given by

$$\bar{\bar{S}}_k = \frac{1}{2}\left[\nabla \vec{v}_k + (\nabla \vec{v}_k)^T\right] - \frac{1}{3} \nabla \cdot \vec{v}_k \bar{\bar{I}}. \qquad (6)$$

This is the same approach taken by Bouillard et al.[14] and Ding and Gidaspow,[17] for example.

2.2 Closure Constitutive Equations

To effect closure, constitutive equations are required for the fluid–particle drag, solids viscosity, and lift forces. In the following, for convenience, we will simplify the discussion to a two-phase fluid–solids situation with the subscript s denoting the solid phase and subscript f denoting the fluid phase. The solids volume fraction is denoted by $\varepsilon_s = (1 - \varepsilon)$ and the fluid volume fraction is denoted by $\varepsilon_f = \varepsilon$.

For the dense region, $\varepsilon \leq 0.8$, the well known Ergun[18] equation (Bird et al.[19] and Kunii and Levenspiel[20]) obtained from packed bed pressure drop data is used to obtain β. In the dilute region, $\varepsilon > 0.8$, β is obtained from the standard drag function for a single sphere

(Bird[19]) corrected empirically by Wen and Yu[21]. The transition between these two expressions is made at a porosity of 0.8. These expressions may be summarized as follows:

$$\beta = \begin{cases} 150\,\dfrac{(1-\varepsilon)^2\mu_f}{\varepsilon\left(d_p\phi_s\right)^2} + 1.75\,\dfrac{\rho_f|\vec{v}_f - \vec{v}_s|(1-\varepsilon)}{d_p\phi_s} & \varepsilon \le 0.8 \qquad (7) \\ \dfrac{3}{4}\,C_d\,\dfrac{\varepsilon|\vec{v}_f - \vec{v}_s|\rho_g(1-\varepsilon)}{d_p\phi_s}\,\varepsilon^{-2.70} & \varepsilon > 0.8 \qquad (8) \end{cases}$$

$$C_d = \begin{cases} 24\left(1 + 0.15\ \mathrm{Re}^{0.687}\right)/\mathrm{Re} & \mathrm{Re} \le 1000 \qquad (9a) \\ 0.44 & \mathrm{Re} > 1000 \qquad (9b) \end{cases}$$

The Reynolds number is given by

$$\mathrm{Re} = \frac{|\vec{v}_f - \vec{v}_s|d_p\phi_s\rho_f\varepsilon}{\mu_f}. \qquad (10)$$

Equations 7-10 have been used to compute fluidization characteristics. Previously computed velocity profiles, bubble shapes and sizes at low and high pressures have agreed with experiments.[22] Therefore, there was felt to be no need to modify β for calculations involving slurries.

The fluid viscosity, μ_f, is taken to be a constant for isothermal flow. The solids viscosity μ_s, is obtained from Krieger's[23] empirical expression for the reduced viscosity, η_r, given by

$$\eta_r = \frac{\varepsilon_s\mu_s + \varepsilon_f\mu_f}{\mu_f} = \left[1 - \frac{\varepsilon_s}{0.68}\right]^{-1.82}. \qquad (11)$$

This expression was used by Phillips et al.[24] in their analysis of concentrated suspension data.

The coulombic stress given in Eq. 3 has been neglected in this paper since this term is usually taken to be zero at and above minimum fluidization conditions as is the case for the data of Altobelli et al.[1] and Sinton and Chow[2].

The sum of the fluid and solids lift force add to zero according to

$$\vec{F}_{fL} + \vec{F}_{sL} = 0 \qquad (12)$$

and the convention is that

$$\vec{F}_{fL} = -\vec{F}_L;\ \vec{F}_{sL} = +\vec{F}_L \qquad (12a)$$

Added to COMMIX-M are two forms of the shear lift (or "slip-shear"[25]) lift force models[26,27]. Such terms account for migration of particles due to a velocity gradient in the fluid.

Saffman's[26] single particle shear lift expressions was extended to a continuum and is given by

$$\vec{F}_L = \frac{6.17}{d_p}(1 - \varepsilon)(\rho_s\mu_s)^{1/2}(\vec{v}_f - \vec{v}_s) \cdot \bar{\bar{S}}_f\left(\overline{\overline{2S}}_f:\bar{\bar{S}}_f\right)^{-1/4}. \quad (13)$$

The shear lift expression due to Drew and Lahey[27] for a sphere in a rotating and straining flow is given by

$$\vec{F}_L = 2C_{vm}(1 - \varepsilon)\rho_f(\vec{v}_f - \vec{v}_s) \cdot \frac{1}{2}\bar{\bar{S}}_f \quad (14)$$

where $C_{vm} = 1/2$ based upon the work of Davidson.[28]

The Saffman lift force was used in all the computations contained in this paper since the carrier fluids used in the experiments analyzed in this paper are highly viscous.

2.3 Boundary Conditions

To solve the three-dimensional equations of fluid-solids flow given above, we need appropriate initial conditions and boundary conditions for the two-phase velocities, the fluid-phase pressure, and the volume fraction. The initial conditions depend upon the problem investigated. The inlet conditions are usually given. The boundary conditions at planes of symmetry demand zero normal gradient of all variables.

At an impenetrable solid wall, the fluid-phase velocities in the three normal and tangential directions are set to zero. The no-slip condition cannot always be applied to the solids phase. Since the particle diameter is usually larger than the length scale of the wall surface roughness, particles may slip along the wall. This mean slip velocity is given by

$$v_{s2}|_w = -\lambda_p \left.\frac{\partial v_{s2}}{\partial x_1}\right|_w, \quad (15)$$

where the x_1 direction is normal to the wall and the x_2 direction is tangential to the wall. The slip parameter, λ_p, is taken to be the mean distance between particles and can be obtained from the expression[29]

$$\lambda_p = \frac{\sqrt{3\pi}}{24}\frac{d_p}{\varepsilon_s g_0}, \quad (16)$$

where

$$g_0 = \left(1 - \frac{\varepsilon_s}{0.65}\right)^{-1.625} \quad (17)$$

is the radial distribution function. Note the close similarity between Eq. 17 and Eq. 11 for the mixture reduced viscosity.

3. Comparison with Experimental Data

Analyses and comparisons of model calculation with the Altobelli et al.[1] and Sinton and Chow[2] NMR data are presented in this section.

3.1 Altobelli et al. Experiment

The Altobelli et al.[1] experiments consisted of a suspension of negatively buoyant divinyl-benzene styrene copolymer (plastic) spheres having a mean diameter of 0.762 mm and a narrow size range (between 0.685 and 0.838 mm), and a density of 1030 kg/m^3 flowing in a horizontal 2.54 cm i.d. acrylic plastic tube which is straight for approximately 2.2 m upstream of the test section. The carrier fluid was 80W oil (gear lubricant) having a density of 875 kg/m^3. NMR concentration and velocity data were taken over a range of 0 to 39 volume percent plastic spheres and average fluid velocities from 1.7 to 22.3 cm/s using a 1.89T superconducting solenoid and a "birdcage" probe tuned to the proton resonant frequency of 80.33 MHz. For details of the NMR technique, the reader is referred to Caprihan et al.[10] and Majors et al.[11]

These suspensions were circulated by a variable speed motor connected to a centrifugal pump. Sections of flexible tygon tubing were used to connect the horizontal acrylic tube to the pump. For further details of the experiment, refer to Altobelli et al.[1]

The velocity and fluid volume fraction data for the 12 runs A1-A3, B1-B3, C1-C3, and D1-D3 published therein for 0, 9, 21 and 39 volume fraction solids were transmitted to ANL on floppy disc to facilitate accurate comparisons with the COMMIX-M computations. The Reynolds numbers based upon the tube diameter and carrier fluid viscosity and density ranged from roughly 1 to 20, and the corresponding estimated entrance lengths were approximately 0.3 to 3 cm. The data were length-averaged along a roughly 2 cm thick slice to increase the signal-to-noise ratio since it was found that concentration and velocity variations in the axial direction ceased (to within the measurement accuracy) before the end of the test section.

Several COMMIX-M meshes were used during the analyses to assess the accuracy of the results based upon the single-phase flow velocity measurements. It was determined that 10 nodes in the radial direction were sufficient to yield fully developed velocity profiles that compared well with the analytical solution as shown in Fig. 1. For this comparison, six nodes were used in the azimuthal direction and 18 in the axial direction using a length of 1.82 m. The results from COMMIX-M and the analytical solution are indistinguishable in the Fig. 1, with computed results being just slightly lower. All of the azimuthal planes gave the same results since gravity was set to zero.

Also shown in Fig. 1 is the experimentally determined single-phase velocity profile for Run A1 having an average velocity of 4.85 cm/s and a maximum velocity of 9.59 cm/s. This velocity profile is for a horizontal slice containing the maximum velocity. As can be seen, the agreement between COMMIX-M, the analytical solution and the data are in excellent agreement in the range ($1.0 \geq r/R \geq -0.5$). Below $r/R = -0.5$, an asymmetry is seen to be present in the data and the data departs further from the analytical solution and COMMIX-M, until at $r/R = -1.0$, the departure is a maximum. Similar, but smaller discrepancies were found to exist between the data and the analytical solution at higher fluid velocities as shown by Altobelli et al.[1] for an average velocity of 21.6 cm/s for Run A3.

The concentration data for this single-phase run are also shown in Fig. 1. Ideally the profile should be a step function, with a maximum fluid volume fraction equal to 1.0 for ($1.0 \geq r/R \geq -1.0$). As can be seen, the maximum value is above 1.0 and peaks at 1.09 at the tube center. There is a falling off near the tube walls as well as an asymmetry. These uncertainties, in part caused by the broadening introduced when the data were filtered to enhance the signal to noise ratio, make it difficult to assess the pipe diameter and should be taken into account to estimate the probable uncertainties in the two-phase velocity and concentration data. Values of porosity greater than 1.0 were seen to exist in the data at the lower solids loading and velocities as well.

For the two-phase runs, which take longer to compute than the single-phase runs, symmetry was assumed about the vertical center line. A total of 8 azimuthal nodes were used for this half plane, 9 in the radial direction and 20 in the axial direction. Uniform fluid volume fraction and equal solids and fluid velocities set equal to the average fluid velocity were used at the pipe inlet, even though these conditions were not achieved in the experiments, in all probability. The initial conditions used were the same as the inlet boundary conditions. Our computational studies showed that nonuniformities of this inlet boundary condition can have a significant effect upon the computed results. This kind of study was not performed in the experiment. The initial conditions have no effect except to change the number of time steps to achieve steady state.

Fig. 2 shows the comparison of the computed and experimental velocity and concentration profiles for run B3, having 9 percent solids volume fraction, and average fluid velocity of 19.3 cm/s. The top two figures are for a horizontal plane containing the maximum experimental velocity, 39.2 cm/s. As can be seen, there is excellent agreement with the data when one takes into account the probable error bounds from Fig. 1. The data show some asymmetry, as shown in Figs. 2a and 2b. COMMIX-M overpredicts the maximum velocity at the tube center as shown in Fig. 2a, but agrees everywhere else. As shown in Fig. 2b, COMMIX-M predicts a slight solids depletion at $r/R = \pm 0.9$. The data also indicate this trend, but taking Fig. 1 into account, the fluid volume fraction data in this region is subject to significant error.

Comparison of the predictions with the experimental velocity and concentration profiles in the vertical plane containing the maximum velocity also reveals excellent agreement with the data for Run B3, as shown in Figures 2c and 2d. The effect of gravity upon the particles is clear with COMMIX-M showing more settling than the data.

Fig. 3 for Run C3, also shows excellent agreement with the data with very similar trends as shown in Fig. 2 for Run B3. The average velocity in this case is 22.3 cm/s and the average solids volume fractions is 21 per cent vs. 9 per cent for Run B3.

3.2 Sinton and Chow Experiment

The Sinton and Chow[2] experiments consisted of a suspension of neutrally buoyant, poly (methyl metracrylate) (PMMA) (Lucite 47G) spheres having a median volume diameter of 0.131 mm with a standard deviation of 0.051 mm flowing in vertical pipes having diameters of 15.2, 25.4 and 50.8 mm and a 500 mm entrance length, which is shorter than the Altobelli et. al. experiment. Intensity and velocity data were taken over a range of 21 to 52 volume percent plastic spheres and Reynolds numbers ranging from 0.005 to 4.0. The carrier fluid was a mixture of polyether oil (Uncon oil, 75-H-90,000), water, and sodium iodide to increase the fluid density to that of the solids having a density of 1190 kg/m^3.

NMR data were taken using a vertically oriented 4.7T superconducting solenoid using techniques developed by Kose et al.[9] and Majors et al.[11]. A positive placement Moyno pump was used.

Three runs are analyzed in this paper 1) 21 percent solids volume fraction, an average fluid velocity of 22.7 cm/s, pipe diameter 2.54 cm. 2) 40 percent solids volume fraction, an average fluid velocity of 17.7 cm/s, pipe diameter 1.52 cm, and 3) 52 percent solids volume fraction, an average fluid velocity of 28.2 cm/s pipe diameter also 1.52 cm. The tube was modeled in two dimensions assuming azimuthal symmetry. A total of 10 nodes were used in the radial direction and 25 in the axial direction.

Comparisons of the computed velocities with the data are shown in Figure 4. As can be seen, excellent agreement exists between the predictions and the data. The velocities near the tube center are slightly overpredicted for the 40 and 52 percent solids volume fraction cases which exhibited slight shear thinning. The maximum velocity near the center for the 21 percent solids volume fraction are slightly underpredicted. This case exhibited basically Newtonian behavior.

It should be noted that the two 21 percent solids volume fraction runs of Altobelli et al.[1], Figure 3, and Sinton and Chow[2], Figure 4a, have very near the same velocity (22.3 cm/s and 22.7 cm/s, respectively). However, the particle size in the latter experiment is smaller (0.131 mm vs. 0.762 mm), so the maximum velocity is higher because the interphase drag is higher. Of course, no gravity effects are evident because the particles are neutrally buoyant. It should also be noted that this experiment did not measure the solids concentration distributions for reasons which are not clear. We assume that the fluid velocity data are correct.

4. Conclusions and Future Plans

Based upon the agreement between the COMMIX-M, computer code predictions and the experimental data, the preliminary constitutive relationship discussed in Sec. 2.2 and boundary condition described in Sec. 2.3 appear to be reasonable and promising. Thus far, no adjustments in the model constants have been made. Further model improvements should increase our confidence in predicting design and processing of dense slurry flow systems. Such model improvements will result from additional comparisons with a wider data base of experimental measurements and COMMIX-M analyses which will also serve to more critically evaluate the models. For example, the solids velocity profiles, overall pressure drops, and pressure distribution should be measured. Inlet boundary conditions of both solids velocity and concentration distributions or, equivalently, any dependence of the measured distributions as a function of entrance length should also be measured to supply input to the computer model; up to now, the assumptions of uniform and equal inlet velocity and uniform concentration distributions have been used. Finally, the rheological properties of suspension flows, especially for shear-thinning, should be examined and studied. The suspension rheological models will then be upgraded to enhance the predictive power of the COMIX-M computer program.

Acknowledgements

The stimulating and constructive discussions and comments of Dr. Jacques X. Bouillard, Energy Systems Division, Drs. Tai H. Chien and Henry M. Domanus, Materials and Components Technology Division, and Professor Shao-Lee Soo, University of Illinois at Urbana-Champaign, are gratefully acknowledged.

The authors want to acknowledge the encouragement from our program manager, Dr. William C. Peters, U.S. Department of Energy, Pittsburgh Energy Technology Center, Drs. Steve Passman, Sandia National Laboratory, and Z. Y. Chen, Science Applications International Corp.

Nomenclature

d_p	Particle diameter, m
$\vec{F}_{kL}$	Shear lift force of phase k, kg/(m^2.s^2)
g	Acceleration due to gravity, m/s^2
$\bar{\bar{I}}$	Unit tensor

M	Number of phases
P	Pressure, Pa
$\bar{\bar{S}}_k$	Strain rate tensor of phase k defined by Eq.(6), Hz
$\vec{v}$	Velocity vector, m/s
$\vec{v}_k$	Velocity of phase k, m/s
$\lvert\vec{v}\rvert$	Magnitude of velocity vector, m/s

Greek Letters

β	Fluid-particle drag coefficient, $kg/(m^3.s)$
δ_{ksi}	Kroenecker delta function; = 1, $k = s_i$; = 0 $k \neq s_i$
ε	Fluid volume fraction
ε_k	Volume fraction of phase k
ε_s	Solids volume fraction = $1 - \varepsilon$
μ_k	Microscopic viscosity, Pa.s x 10 = poise
ρ_k	Density of phase k, kg/m^3
ρ_s, ρ_f	Solids and fluid phase densities, respectively, kg/m^3
$\bar{\bar{\tau}}_{kc}$	Co ılombic stress for solids ($k = s_i$), Pa
$\bar{\bar{\tau}}_{ke}$	Effective phase stress tensor, defined by Equation (5), Pa
$\bar{\bar{\tau}}_{kv}$	Microscopic viscous phase stress tensor, Pa
ϕ_S	Sphericity of particles (shape factor); $0 < \phi_S \leq 1$

Subscripts

f	Fluid phase
k	Phase k
s_i	Solids phase i

Superscripts

$\rightarrow$	Denotes a vector quantity
$=$	Denotes a tensor quantity

Operator

$\nabla\bullet$	Divergence
∇	Gradient

References

1. Altobelli, S. A., R. C. Givler, and E. Fukushima, *Velocity and Concentration Measurements of Suspensions by Nuclear Magnetic Resonance Imaging*, J. Rheology, 35, (5), pp 721–734 (1991).

2. Sinton, S. W. and A. W. Chow, *NMR Flow Imaging of Fluids and Solid Suspensions in Poiseuille Flow*, J. Rheology, 35, pp. 735–772 (1991).

3. Bedford, A. and D. S. Drumheller, *Theories of Immiscible and Structured Mixtures*, Int. J. Eng. Sci., 21, pp. 863–960 (1983).

4. Graham, A. L. and R. B. Bird, *Particle Clusters in Concentrated Suspensions. 1. Experimental Observations of Particle Clusters*, Ind. Eng. Chem. Fund., 23, pp. 406–410 (1984).

5. Graham, A.L. and R.D. Steele, *Particle Clusters in Concentrated Suspensions.* 2. Information Theory and Particle Clusters, 23, pp. 411–420 (1984).

6. Graham, A.L., R.D. Steele, and R.B. Bird, *Particle Clusters In Concentrated Suspensions. 3. Prediction of Suspension Viscosity*, 23, pp. 420–425 (1984).

7. Wendt, R E., P.H. Murphy, J.J. Ford, R.N. Bryan, and J.A. Burdine, *Flow and Motion in NMR Imaging: A Tutorial Introduction*, in Technology of Nuclear Magnetic Resonance, pp. 121–135, The Society of Nuclear Medicine, New York, 1984.

8. Caprihan, A., and E. Fukushima, *Flow Measurements by NMR*, Phys. Rev. 198, pp. 195–235 (1991).

9. Kose, K., K. Satoh, T. Inouye, and H. Yasuoka, *NMR Flow Imaging*, J. Phys. Soc., Japan 54, pp. 81–92 (1985).

10. Caprihan, A., J.G. Davis, S.A. Altobelli, and E. Fukushima, *A New Method for Flow Velocity Measurement: Frequency-Encoded NMR*, Magn. Reson. Med. 3, pp. 352–362 (1986).

11. Majors, P.D., R.C. Givler, and E. Fukushima, *Velocity and Concentration Measurements in Multiphase Flows by NMR*, J. Magn. Reson. 85, pp. 235–243 (1989).

12. Domanus, H.M., W.T. Sha, V.L. Shah, J.G. Bartzis, J.L. Krazinski, C.C. Miao, and R.C. Schmitt, *COMMIX-2: A Steady/Unsteady Single-Phase/Two-Phase Three-Dimensional Computer Program For Thermal-Hydraulic Analysis of Reactor Components*, NUREG/CR-1807, Argonne National Laboratory Report ANL-81-10, Argonne, IL (October 1980).

13. Sha, W.T., B. T. Chao, and S.L. Soo, *Local Volume-Averaged Transport Equations for Multiphase Flow in Regions Containing Distributed Solid Structures*, NUREG/CR-2354, Argonne National Laboratory Report ANL-81-69 Argonne, IL (December 1981).

14. Bouillard, J.X., R.W. Lyczkowski, D. Gidaspow, and G.F. Berry, *Hydrodynamics of Erosion of Heat Exchanger Tubes in Fluidized-Bed Combustors*, Canadian J. Chemical Engineering, 67, pp. 218-229 (April 1989).

15. Bouillard, J.X., R.W. Lyczkowski, and D. Gidaspow, *Porosity Distributions in a Fluidized Bed with An Immersed Obstacle*, AIChEJ. 35, No. 6, pp. 908-922 (June 1989).

16. Lyczkowski, R.W., J.X. Bouillard, D. Gidaspow, and G.F. Berry, Hydrodynamics of Fluidization: Time-Averaged and Instantaneous Porosity Distributions in a Fluidized Bed with an Immersed Obstacle, Argonne National Laboratory Report ANL/ESD/TM-4, Argonne, Illinois, September 1986 (published February 1990).

17. Ding, J. and D. Gidaspow, A. *Bubbling Fluidization Model Using Kinetic Theory of Granular Flow*, AIChE J., 36. No. 4, pp. 523-530 April 1990).

18. Ergun, S., *Fluid Flow Through Packed Columns*, Chemical Engineering Progress 48(2), pp. 89-94 (1952).

19. Bird, R.B., W.E. Stewart and E.N. Lightfoot, *Transport Phenomena*, (3rd Printing), John Wiley, New York (1960).

20. Kunii, D., and O. Levenspiel, *Fluidization Engineering, John Wiley and Sons, Inc., New York (1969)*

21. Wen, C.Y., and Y.H. Yu, *Mechanics of Fluidization*, B. S. Lee ed., AIChE Symp. Series 62, (62), pp. 100-112, American Institute of Chemical Engineers, New York (1966).

22. Gidaspo,w, D., *Hydrodynamics of Fluidization and Heat Transfer: Supercomputer Modeling, Applied Mechanics Review*, 39(1), pp.1-23 (January 1986).

23. Krieger, I.M., *Adv. Colloid Interface Sci.*, 3, pp. 111 (1972).

24. Phillips, R.J., R.C. Armstrong, R.A. Brown, A.L. Graham and J.R. Abbott, *A Constitutive Equation for Concentrated Suspensions that Accounts for Shear-Induced Particle Migration, Phys. Fluids*, A 4(1). pp. 30-40 (1992).

25. Johnson, G., M. Massoudi, and K.R. Rajagopal, *Flow of a Fluid Infused With Solid Particles Through a Pipe*, Int. J. Eng. Sci., 29, No. 6, pp. 649-661 (1991).

26. Saffman, P.G., *The Lift on a Small Sphere in Slow Shear Flow*, J. Fluid Mech., 22, part 2. pp. 385-400 (1965).

27. Drew, D.A. and R. T. Lahey, Jr., *Application of General Constitutive Principles and the Derivation of Multidimensional Two-Phase Flow Equations*, Int. J. Multiphase Flow, 5, pp. 243-264 (1979).

28. Davidson, M.R., *Numerical Calculation of Two-Phase Flow in a Liquid Bath with Bottom Gas Injection: The Central Plume*, Appl. Math. Modelling, 14, pp. 67-76 (1990).

29. Ding, J., and R.W. Lyczkowski, *Three Dimensional Kinetic Theory Modeling of Hydrodynamics and Erosion in Fluidized Beds*, accepted for publication in Powder Technology (1992).

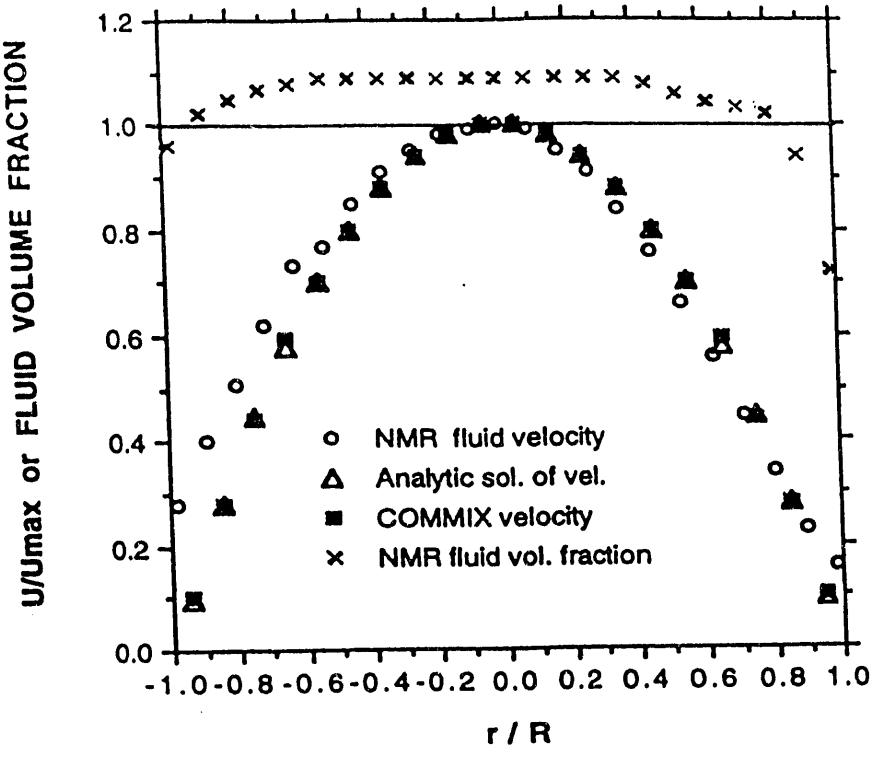

Figure 1. Altobelli, et al.[1] NMR Fluid Velocity and Volume Fraction Data for RUN A1 and Comparison at Experimental Velocity Data With COMMIX-M and Analytic Solution. Pure Fluid Case.

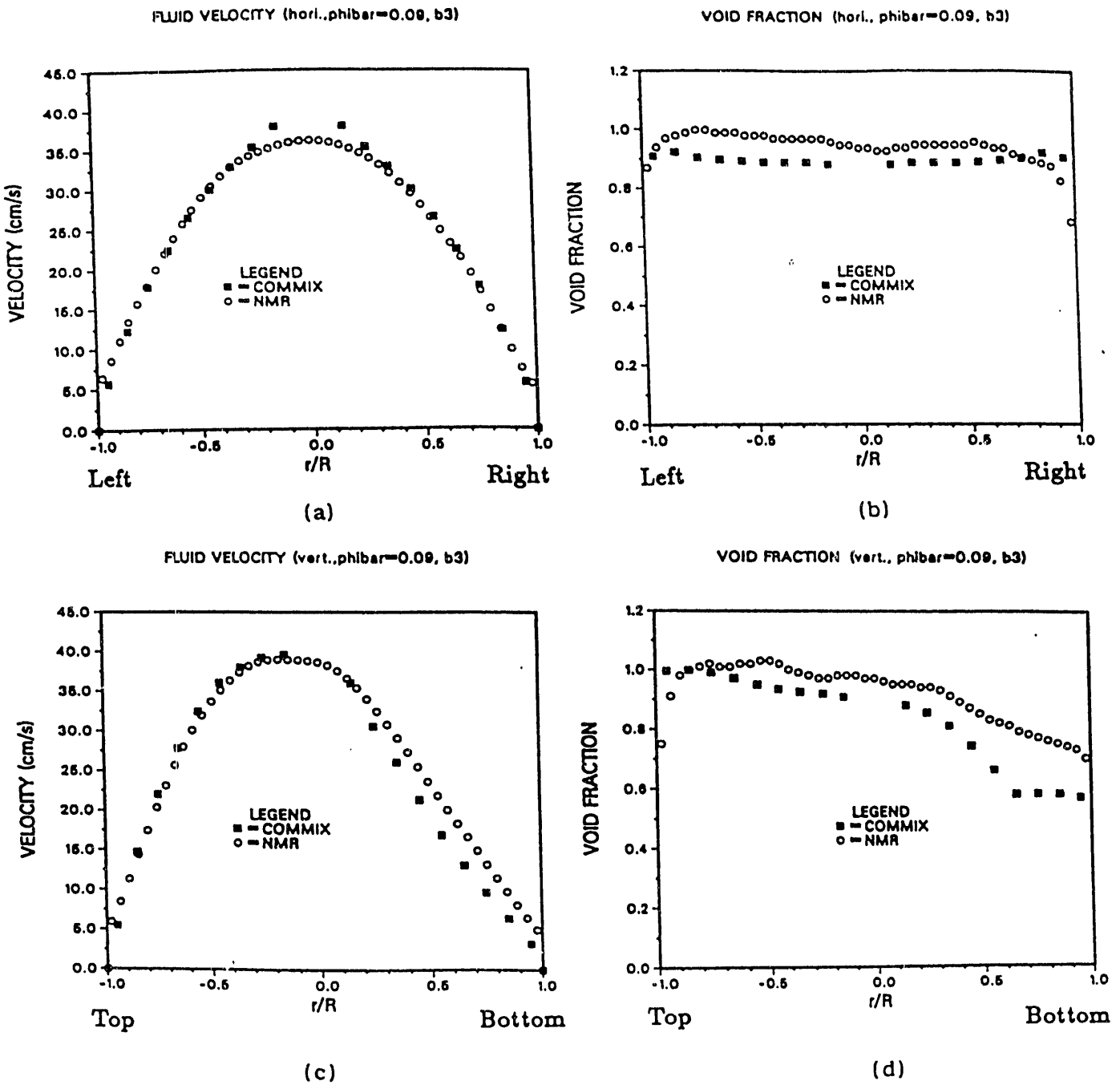

Figure 2. Comparison of Predicted and Experimental Altobelli et al.[1] Data: a) Horizontal Fluid Velocity. b) Horizontal Fluid Volume Fraction. c) Vertical Fluid Velocity. d) Vertical Fluid Volume Fraction. Run B3, 9 % Solids Volume Fraction, Average Fluid Velocity, 19.3 cm/s.

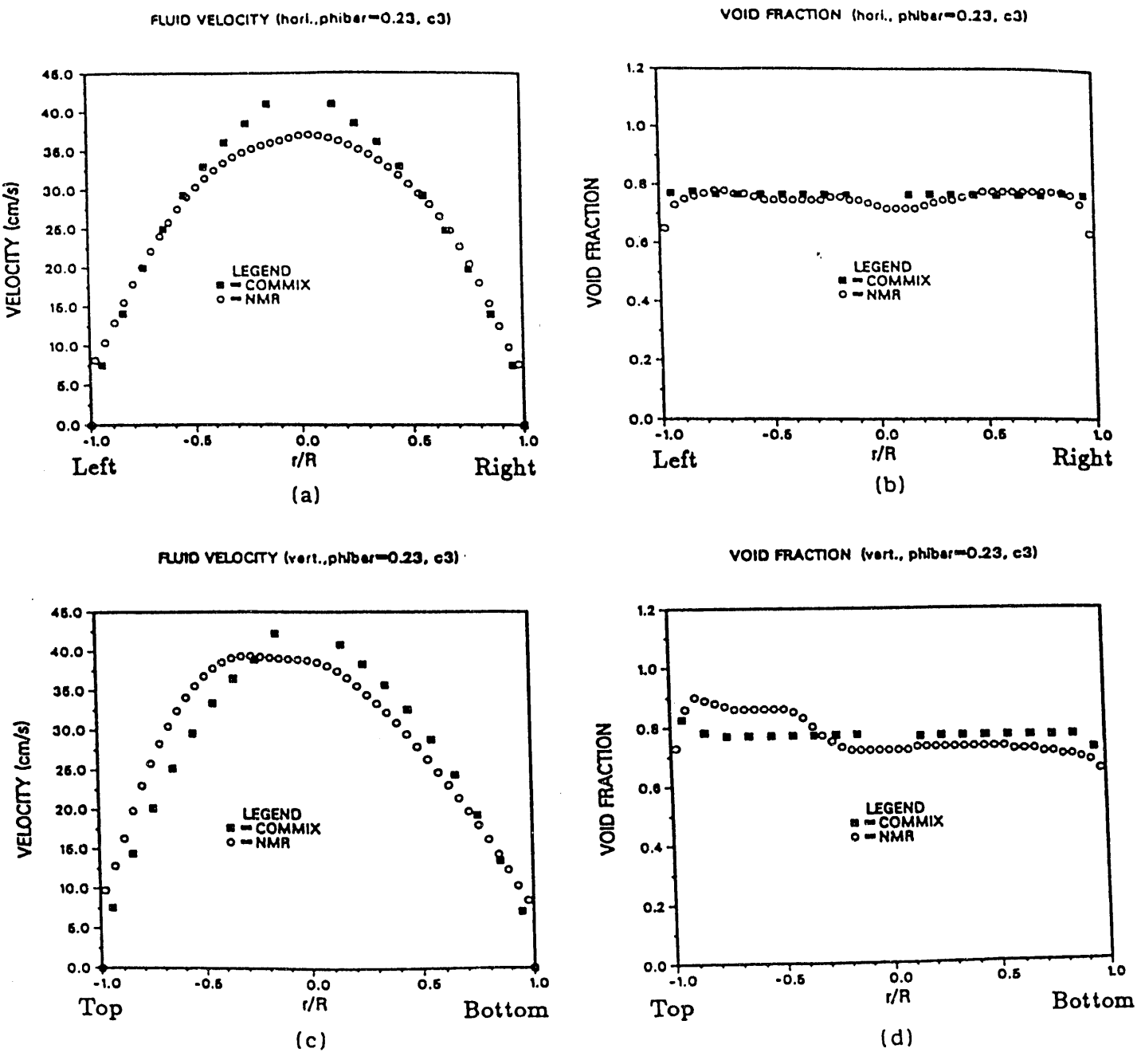

Figure 3. Comparison of Predicted and Experimental Altobelli et al.[1] Data: a) Horizontal Fluid Velocity. b) Horizontal Fluid Volume Fraction. c) Vertical Fluid Velocity. d) Vertical Fluid Volume Fraction. Run C3, 23 % Solids Volume Fraction, Average Fluid Velocity, 22.3 cm/s.

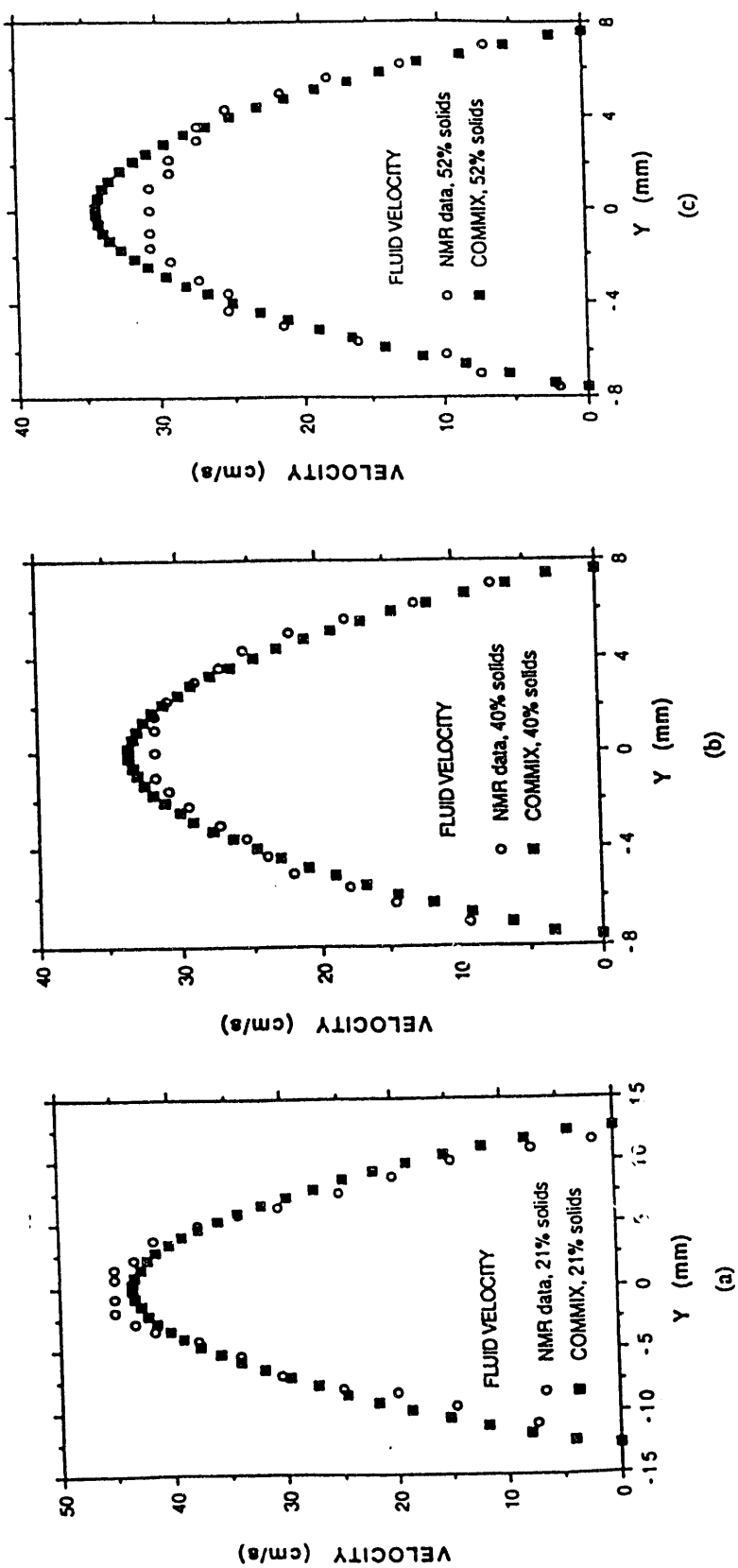

Figure 4. Comparison of Predicted and Experimental Sinton and Chow [2] NMR Velocity Data: a) Average Fluid Velocity 22.7 cm/s, Tube Diameter 2.54 cm/s; b) Average Fluid Velocity, 17.6 cm/s, Tube Diameter, 1.52 cm; c) Average Fluid Velocity, 17.5 cm/s, Tube Diameter 1.52 cm.

END

DATE FILMED

2/5/93